

Dynamics of the Harper map: Localized states, Cantor spectra and Strange nonchaotic attractors

Surendra Singh Negi and Ramakrishna Ramaswamy

School of Physical Sciences

Jawaharlal Nehru University, New Delhi 110 067, INDIA

(November 16, 2018)

Abstract

The Harper (or “almost Mathieu”) equation plays an important role in studies of localization. Through a simple transformation, this equation can be converted into an iterative two dimensional skew–product mapping of the cylinder to itself. Localized states of the Harper system correspond to fractal attractors with nonpositive maximal Lyapunov exponent in the dynamics of the associated Harper map. We study this map and these strange nonchaotic attractors (SNAs) in detail in this paper. The spectral gaps of the Harper system have a unique labeling through a topological invariant of orbits of the Harper map. This labeling associates an integer index with each gap, and the scaling properties of the width of the gaps as a function of potential strength, ϵ depends on the index. SNAs occur in a large region in parameter space: these regions have a tongue–like shape and end on a Cantor set on the line $\epsilon = 1$ where the states are critically localized, and the spectrum is singular continuous. The SNAs of the Harper map are described in terms of their fractal properties, and the scaling behaviour of their power–spectra. These are created by unusual bifurcations and differ in many respects from SNAs that have hitherto been studied. The technique of studying a quantum eigenvalue problem in terms of the dynamics of an associated mapping can be applied to

a number of related problems in 1 dimension. We discuss generalizations of the Harper potential as well as other quasiperiodic potentials in this context.

I. INTRODUCTION

The Harper equation, the discrete Schrödinger equation for a particle in a quasiperiodic potential,

$$\psi_{n+1} + \psi_{n-1} + 2\epsilon \cos 2\pi(n\omega + \phi_0)\psi_n = E\psi_n, \quad (1)$$

was originally introduced in the study of the motion of an electron in two dimensional lattice in a magnetic field [1]. In the above equation, ψ_n is the wavefunction at lattice site n , ω is an irrational number, and ϕ_0 is a parameter. The nature of the eigenfunctions and the eigenspectrum has been of considerable interest since this equation arises in numerous and varied contexts [2–7].

Studies of localization phenomena have been important in condensed matter physics research for more than forty years [8], and here the Harper system has played a very important role. In systems with a periodic potential, the Bloch theorem holds and leads to wavefunctions which typically are extended. In the contrasting case of a random potential, the states are localized. A quasiperiodic potential is intermediate between these limits, and it is of interest to determine whether states are localized or extended. Indeed, the problem of localization has important implications in a variety of fields, among the most significant being an explanation of transport properties in disordered solids [2–8] (for example the Mott theory of the metal–insulator transition [9]). In a 1-dimensional tight-binding model with incommensurate modulation, at a critical strength of potential there exists a metal insulator transition. Such a quasiperiodic system is physically realizable, for instance, in quasicrystals which have incommensurate modulation and therefore lack translational order [10]).

As is evident, the Harper equation is invariant under the transformation $\psi_n \rightarrow (-1)^n\psi_n, \epsilon \rightarrow -\epsilon, E \rightarrow -E$, so that it suffices to consider the case E, ϵ nonnegative. A

number of studies [6,10–17] have examined different properties of the eigenstates and spectrum of the Harper equation. The most important feature of this system is that for $\epsilon = 1$, the equation is self–dual [17]: the equation for the Fourier transform of ψ_n is identical to Eq. (1). The quantum eigenstates are extended for $\epsilon < 1$, exponentially localized for $\epsilon > 1$ and but at the *critical* value $\epsilon = 1$, the states are power–law localized. The eigenvalue spectrum is singular–continuous (namely, the spectrum forms a Cantor set) for all irrational values of ω at this critical value of ϵ [4]. For rational values of ω , the Bloch theorem applies, and leads to a spectrum consisting of bands.

In a study of the continuous version of Eq. (1), namely

$$-\frac{d^2\psi(x)}{dx^2} + 2\epsilon \cos(2\pi\omega x)\psi(x) = E\psi(x), \quad (2)$$

Bondeson, Antonsen and Ott [18] pointed out that by using Prüfer’s transformation, the above Schrödinger equation could be converted into an ordinary differential equation for the variable $y = \tan^{-1}(2g\psi'\psi)/((\psi')^2 - g^2\psi^2)$, g being an arbitrary constant, as

$$\frac{dy}{dx} = \frac{1}{g}\{[g^2 + k^2(x)] + [g^2 - k^2(x)] \cos y\} \quad (3)$$

where $k^2(x) = E - 2\epsilon \cos(2\pi\omega x)$. This equation describes a forced dynamical system (the independent variable x is now the “time”), the forcing term deriving from the potential being quasiperiodic if ω is irrational. Study of the orbits of Eq. (3) gives information on the behaviour of wave–functions of Eq. (2). Indeed, the Lyapunov exponent λ for an orbit of the dynamical system is related to the localization length γ of the corresponding wavefunction [18],

$$\lambda = -2/\gamma. \quad (4)$$

Thus localised states($\gamma > 0$) correspond to attractors with negative Lyapunov exponents, while extended states ($\gamma \rightarrow \infty$) correspond to orbits with zero Lyapunov exponent. As Bondeson *et al.* [18] further argued, the quasiperiodic driving precluded the possibility of a simple structure for these attractors, which were both fractal and had nonpositive Lyapunov exponents: these are strange nonchaotic attractors (SNAs) [19].

Our concern in this paper is the dynamics of the Harper mapping which is a similar transformation of Eq. (1), using Riccati variables, namely $\psi_{n-1}/\psi_n \rightarrow x_n$ [20,21]. Eq. (1) becomes the two-dimensional mapping

$$x_{k+1} = -[x_k - E + 2\epsilon \cos 2\pi\phi_k]^{-1} \quad (5)$$

$$\phi_{k+1} = \phi_k + \omega \quad \text{mod } 1. \quad (6)$$

While this is exactly equivalent to the Harper equation, it is amenable to somewhat simpler analysis since boundary conditions that must be imposed for quantization in Eq. (1) become conditions on the dynamical state of orbits in the mapping, Eqs.(5-6).

Viewed merely as an iterative mapping of the plane, the above system has several features of interest. The map is reversible, so there can be no chaotic dynamics, but for sufficiently large ϵ , it can be argued [22] that there must be an attractor of the dynamics which has an infinite set of discontinuities. The attractors are therefore both strange (i.e. fractal) and nonchaotic (the Lyapunov exponents must be nonpositive): they are SNAs. The Harper map is another example of a quasiperiodically forced nonlinear dynamical system where it is known that SNAs are frequently encountered [23]. By now a variety of quasiperiodically driven systems with SNA dynamics are known; these include examples of driven pendulums, forced nonlinear maps, the driven van der Pol oscillator, neural network systems, as well as some mappings where there is no explicit quasiperiodic driving [23]. Owing to the fractal structure of the attractors, the dynamics is strictly aperiodic, but the correlation properties [24] of SNAs show them to be much less aperiodic than chaotic attractors, the correlation function always lying between 0 and 1.

Strange nonchaotic dynamics is of considerable interest since it is intermediate in several ways between regular and chaotic motion. SNAs are typically found in the region of a transition to chaos, and several routes or scenarios for their formation are now known [23]. Their existence can be confirmed by explicit calculation of Lyapunov exponents and fractal dimensions, or by computing their spectral and correlation properties. In the Harper system it is known that SNAs can be created by the homoclinic collision of an invariant curve with

itself [25], and that this route to SNA is accompanied by an unusual symmetry breaking. There are other routes through which SNAs can also be formed, and some of these are described here as well.

The Harper system is therefore of interest from both the nonlinear dynamics perspective, as well as in the context of localization. Indeed, as initial studies have shown [22,25,26], both these aspects of the problem are related, and the correspondence between SNAs and localized states can be exploited so as to provide new insights in the study of forced nonlinear systems, as well as for localization studies. It has been noted for instance, that quasiperiodic potentials are frequently associated with critical or power-law localized states, just as quasiperiodic driving frequently transforms chaotic attractors to SNAs. This can be made more concrete by studying the iterative mappings analogous to Eqs. (5-6) that are associated with such potentials. In many instances, it also turns out that such systems have attractors which are SNAs [27].

This paper is concerned with such correspondences. One focus is on what can be learned about the spectrum and eigenstates of the Harper equation through a study of the dynamics of the Harper map. At the duality point, $\epsilon = 1$, the eigenspectrum is given exactly by the zeros of the Lyapunov exponent, $\lambda(E)$. Furthermore, topological properties of the orbits of the mapping provide a unique labeling of the gaps in the spectrum. The gap indices also determine the scaling behaviour of the gaps as a function of the coupling constant [26]. These results are described in Section III of this paper. The behaviour of the gaps as a function of coupling constant is important for a number of problems, and we have shown [26] how the gaps can be uniquely labeled by mapping them on to a Cayley tree. The gap labels are winding numbers, which are topological invariants for orbits of the iterative mapping. These determine the scaling behaviour of the gaps at, above, and by duality, below, the critical coupling, $\epsilon = \epsilon_c \equiv 1$. We discuss the general scheme for labeling the gaps for particular choices of ω such as the golden mean or silver mean ratios, as well as for other algebraic and transcendental irrational ratios.

At the same time, the SNAs of the Harper map are themselves of interest. Regions (in parameter space) where they occur have an interesting hierarchical geometry, being organized in fractal “tongue–like” zones [26]. In Section II of this paper, we first describe properties of the iterative mapping for the Harper potential. The phase diagram for this system, as a function of E and ϵ for fixed irrational ω is discussed. The different bifurcation routes for the formation of SNAs, and the measures have been introduced in the past few years in order to distinguish SNAs from other related attractors are elaborated in Section IV.

The case of quasiperiodic potentials obtained by generalizing the Harper potential, where critical states are known to occur, are discussed in Section V. We show that the technique of determining the spectrum from the behaviour of the Lyapunov exponent versus parameter curve can be extended to these potentials as well. Other cases of systems with critical states are known, as for example the quasiperiodic potentials that arise from the Fibonacci, Thue–Morse, Rudin–Shapiro and period–doubling symbolic sequences. The corresponding iterative mappings also support SNAs [28]. The paper concludes with a summary in Section VI.

II. THE HARPER MAP

We study the mapping Eqs. (5-6) and other quasiperiodic generalizations of it which arise from quasiperiodic Schrödinger problems. While most of the essential features of the system do not depend on the precise value of ω so long as it is irrational, some of the details (such as the arrangements of the gaps, see Section III below) do. In this work ω is taken to be a quadratic irrational number such as the golden mean ratio $(\sqrt{5} - 1)/2$, which is the value for which most previous studies have been carried out, or the silver mean ratio, $\sqrt{2} - 1$.

The Harper map is a skew–product dynamical system on the cylinder $\mathbf{S}^1 \otimes \mathbf{R}$. Since the ϕ dynamics is quasiperiodic, there are no periodic orbits. There is also no chaotic dynamics. In general there are three qualitatively different types of motion that can occur in this

system. There can be quasiperiodic tori (two–frequency or three–frequency) with negative Lyapunov exponent, neutrally stable curves with zero Lyapunov exponent, when the phase space is conserved under the flow, and strange nonchaotic dynamics. On SNAs the motion is both aperiodic and, as is characteristic of such attractors, intermittent [29].

The ϕ - freedom is neutral with the corresponding Lyapunov exponent being trivially zero, while for the x - freedom, the stretch exponent or one–step Lyapunov exponent [30] is

$$y_i = \ln |x'_{i+1}| = 2 \ln |x_{i+1}|. \quad (7)$$

The N -step finite–time Lyapunov exponent is

$$\lambda_N(x_i) = \frac{1}{N} \sum_{j=0}^{N-1} y_{j+i}. \quad (8)$$

These local exponents are indexed by initial condition x_i , but the asymptotic Lyapunov exponent,

$$\lambda = \lim_{N \rightarrow \infty} \lambda_N(x_i), \quad (9)$$

is independent of (almost every) initial condition. In the rest of the paper, we deal only with this nontrivial Lyapunov exponent, for which the following relation holds [11,17],

$$\lambda(E, \epsilon) = -2 \ln(\epsilon) + \lambda(1/\epsilon, E/\epsilon). \quad (10)$$

relating the exponents above and below the critical coupling.

The eigenvalue E appears simply as another parameter in the Harper map. Quantization conditions that apply for the Harper equation, namely that the wavefunctions should be normalizable, now become conditions on the dynamical state of the map. In particular, these can be viewed as conditions on the Lyapunov exponents: for extended states the Lyapunov exponent is zero, while for localized states, the Lyapunov exponent is negative.

At the duality point ϵ_c , eigenstates of the Harper equation are critically localized. Hence, the Lyapunov exponent of the Harper map is identically zero whenever E is an eigenvalue. Furthermore, since the spectrum is known to be singular–continuous, the λ versus E curve

meets the line $\lambda = 0$ on a Cantor set of points (Figs. 1a,b). Indeed, the Hofstadter butterfly [4] which is the spectrum of the Harper equation as a function of ω can be determined as the set $\{E : \lambda(E, \omega, \epsilon_c) = 0\}$.

The variation of the Lyapunov exponent with ϵ is simple if E is an eigenvalue. Below $\epsilon = 1$, the exponent is zero and the state is extended, while above it, $\lambda \sim -\ln \epsilon$ and the state is localized; see Fig. 2 for the case of $E = 0$. Of particular note is the discontinuity (in slope) at ϵ_c : the localization transition can therefore be viewed as a bifurcation. As shown previously, this bifurcation is accompanied by a quasiperiodic symmetry-breaking and the homoclinic collision of neutrally stable invariant curves to form a SNA [25]. For other eigenvalues, the location of the eigenvalue changes with ϵ . At ϵ_c there is always a symmetry-breaking, but there need not be the homoclinic collision, so SNAs can be formed here by other routes [31,32] as is discussed in Section IV below.

The overall dynamical behaviour in the Harper map can be summarized in a phase diagram, shown in Fig. 3a for the case of $\omega = \sqrt{2} - 1$, namely the silver mean ratio. Owing to the $E \rightarrow -E$ symmetry, it suffices to consider $(E > 0, \epsilon > 0)$. We compute the Lyapunov exponent and determine the dynamical state in the different regions demarcated in the figures. Below ϵ_c , the dynamics is either on invariant curves (I) or on tori (Q), while above ϵ_c , there are regions of SNA (S) and tori (Q). The SNA regions exist only at and above ϵ_c . As was first argued by Ketoja and Satija [22], in the strong-coupling limit of large ϵ , the dynamics is guaranteed to be on SNAs; this argument can be extended down to ϵ_c . Above ϵ_c , therefore, the dynamics is largely on SNAs. The gap regions extend above ϵ_c . Therefore, by continuity, the SNA regions emanate from the eigenvalues at ϵ_c . These have a tongue-like shape, and since each eigenvalue is associated with one such region, these are hierarchically organized in the same manner as are the energy eigenvalues: SNAs occur in fractal tongues. Shown in Fig. 3b is a (schematic) detail in the neighborhood of one (and therefore of every) tongue: the region of 3-frequency quasiperiodic orbits or tori for $\epsilon < 1$ are mirrored by SNA regions for $\epsilon > 1$.

The major differences between the cases of different ω arise from the manner in which the regions of tori (Q) are arranged. These correspond to gaps in the eigenspectrum of the Harper operator, which we now discuss.

III. GAPS OF THE HARPER SPECTRUM

The eigenvalue spectrum of the Harper equation is singular-continuous for irrational ω at ϵ_c , namely it forms a Cantor set. The nature of the gaps in the spectrum has been of great interest in a number of different contexts in the past several years. In particular, how the gaps behave as a function of the potential strength, namely ϵ , has been a long-standing question [20,33].

The eigenvalues can be simply deduced from the λ versus E curve at ϵ_c , as shown in Fig. 1a for the case of ω the golden mean ratio, or in Fig. 1b for ω the silver mean ratio. The tori regions of the Harper map correspond to gaps in the eigenvalue spectrum of the Harper equation. Orbits for such values of E and ϵ are 1-d curves that wind across the cylinder an integral number of times. Within each gap, this integer index is constant and measures the number of times the orbit crosses the boundaries $x \rightarrow \pm\infty$. This essentially counts the number of changes of sign of the wave-function (per unit length), and is related to a winding number for the orbit. These indices are indicated in Figs. 1a and 1b for the largest visible gaps.

For rational frequencies, the spectrum of the Harper equation consists of a finite number of bands. If $\omega = p/q$, p, q integers, then there are q or $q - 1$ bands depending on whether q is odd or even, and therefore in the positive energy spectrum the number of gaps is $(q - 1)/2$ or $(q/2 - 1)$. For rational ω all orbits are periodic with period q . For energies in the gaps, the orbits form a 1-parameter family, indexed by initial phase, from which the winding number can be easily extracted.

As is well-known [34], an irrational number has a unique continued fraction representation. Thus an irrational frequency

$$\omega \equiv [a_1, a_2, a_3, \dots] = \cfrac{1}{a_1 + \cfrac{1}{a_2 + \cfrac{1}{a_3 + \cfrac{1}{\ddots}}}}$$
(11)

a_i 's integers, can be successively approximated by a unique series of rational approximants. By truncating the continued fraction representation up to the term a_j , one obtains the rational p_j/q_j ; the sequence $p_j/q_j, j = 1, 2, \dots$ converges, $\lim_{k \rightarrow \infty} p_k/q_k \rightarrow \omega$. For a given approximant p_j/q_j , the gap structure of the spectrum can be described in terms of the winding numbers. These run from 1 to $q_j/2 - 1$ or $(q_j - 1)/2$, as discussed in the preceding paragraph. The new gaps that appear for the next approximant, p_{j+1}/q_{j+1} , do not alter the *inter se* ordering of the gaps already present for lower order rational approximants. Thus the gap structure for irrational ω can be deduced by sequentially examining the structure of the gaps for the successive rational approximations to ω . Each gap in the spectrum, or each region of tori in the map, can therefore be uniquely labeled by an integer index.

For algebraic irrationals which have periodic continued fraction representations, there are simplifications that permit a more compact description of the ordering scheme. We now describe this for the case for the golden and silver mean ratios.

The golden mean is the limiting ratio of successive Fibonacci numbers, F_k/F_{k+1} , where F_k is given by the relation

$$F_{k+1} = F_k + F_{k-1}, k = 1, 2, \dots, \text{ with } F_0 = 0, F_1 = 1, \quad (12)$$

the first few being 0, 1, 1, 2, 3, 5, 8, ..., while the silver mean is the limiting ratio of the successive integers of the family 0, 1, 2, 5, 12, 29, 70, ..., namely

$$S_{k+1} = 2S_k + S_{k-1}, k = 1, 2, \dots, \text{ with } S_0 = 0, S_1 = 1 \quad (13)$$

with $\lim_{k \rightarrow \infty} S_k/S_{k+1} \rightarrow \sqrt{2} - 1$.

The ordering of the gaps can be best described by first constructing a graph for the particular irrational ratio in the following manner. We discuss this in detail for the silver mean ratio below, and indicate the analogous result for the golden mean ratio [26].

Consider a Cayley tree, arranged as shown in Fig. 4a, with each node (except the origin, labeled 0) having two successors. Nodes at the same horizontal level are at the same generation. The rightmost node at each generation is labeled by successive S_k , while the leftmost are half the successive even S_k 's. The other integers are identified with the remaining nodes as follows: for given m , the mother node i_m is the smallest available such that

- $m + i_m$ is one of the integers S_k . If i_m already has two daughters, then the mother node is chosen such that
- $m + i_m$ is one of the integers $\bar{S}_{k+1} = S_{k+2} - S_{k+1}$, namely 1,3,7,17,41,...

For ω the golden mean, i_m is chosen such that $m + i_m$ is the smallest possible Fibonacci integer [26]. Complicated (but deducible [26]) rules determine which branch (left or right) the daughters are placed, but the above procedure results in an unique arrangement of all integers on the Cayley tree: see Figs. 4a and 4b.

The actual ordering of the gaps derives from the following additional consideration. Every pair of integers, i_1 and i_2 , with $i_2 > i_1$, has two possibilities as to how they are relatively placed on this graph. Either

1. i_1 is an ancestor of i_2 , i.e. there is a directed path connecting i_2 to i_1 . If this path is to the left at node i_1 , then $i_2 \prec i_1$. (If to the right, then $i_1 \prec i_2$.)
or
2. i_0 is the most recent common ancestor of i_1 and i_2 . If the path from i_0 to i_1 is on the left at i_0 , then $i_1 \prec i_2$. (Similarly, if it is to the right, then $i_2 \prec i_1$.)

This gives a unique ordering of the integers with the relation \prec being transitive (if $i \prec j$ and $j \prec m$ then $i \prec m$). Thus, for the silver mean we get

$$\dots \prec 35 \prec \dots \prec 11 \prec \dots \prec 1 \prec \dots \prec 4 \prec \dots \prec 2 \prec \dots \prec 7 \prec \dots \prec 12 \prec \dots \prec 0.$$

while for the golden mean, the ordering is

$$\dots \prec 4 \prec \dots \prec 9 \prec \dots \prec 1 \prec \dots \prec 7 \prec \dots \prec 2 \prec \dots \prec 11 \prec \dots \prec 21 \prec \dots \prec 0.$$

The gaps appear in precisely this order: if $k \prec \ell$, then the gap with index k precedes the gap with index ℓ in the positive energy spectrum of the Harper system: see Figs. 1a,b where gap labels for the largest visible gaps are indicated. The labels have been determined by examination of orbits of the map as described. The attractor shown in Fig. 5 is an orbit in the gap labeled 8 (which lies between gaps 4 and 3) in the silver-mean Harper system.

As can be seen in Figs. 1a and 1b, each gap has two attributes: the width and the depth. The width is the spacing between two energy eigenvalues of the Harper equation, but the depth has no immediate significance, being just the minimum value that the Lyapunov exponent takes between two zeros. These are denoted w_m and d_m respectively, and both are functions of the coupling strength, ϵ .

In general, both widths and depths decrease with order (i.e. with increasing gap index), and with increasing ϵ . However, and particularly in the case of the widths, the dependence on gap label is nonmonotonic, in a manner described below. The depths scale in a simple fashion, namely

$$d_N \sim \frac{C}{N\epsilon^N}, \quad (14)$$

as shown in Figs. 6a,b. On the other hand, the widths must be considered in *families* labeled along a consistent branch of the Cayley tree. For example, for $\omega = \sqrt{2} - 1$ (see Fig. 4a), the gaps $1, 2, 5, 12, 29, \dots$, the rightmost nodes at each generation form one family, while gaps $1, 6, 35, 204, \dots$, the leftmost nodes, form another family, for each of which the widths scale, at ϵ_c , as

$$w_N \sim \frac{1}{N^\theta}, \quad (15)$$

the exponent θ being particular to a given family of gaps. The two families of gaps enumerated above are the fastest and slowest decreasing, respectively, with exponents $\theta_l \approx 2.05$ and $\theta_r \approx 2.31$. For all other families, the exponents lie within the limits $[\theta_l, \theta_r]$. Similar results for the golden mean case are shown in Fig. 5b.

Wiegmann *et al.* [6] have studied the tight-binding Harper Hamiltonian for which they obtain the gap distribution, namely the number of gaps lying between D and $D+dD$. They

find that this quantity, $\rho(D) \sim D^{-\gamma}$ where γ is found to be approximately $3/2$; similar exponents have been reported by Geisel *et al.* [15] as well. If the gaps are rank-ordered, namely from largest downwards, disregarding the gap indices, then we observe that they decrease as

$$w_r \sim \frac{1}{r^\mu}. \quad (16)$$

$\mu \approx 2$, which is consistent with the power-laws obtained earlier [6,15].

IV. SNAS IN THE HARPER SYSTEM

We now turn to the description of the dynamical attractors in the Harper map. Strange nonchaotic dynamics in the Harper system is known to be created through a number of different routes or scenarios. Unlike other examples of quasiperiodically forced systems wherein SNAs are formed by mechanisms that have parallels with routes to chaos in similar unforced systems, here the routes to SNA can be quite distinctive.

A. Homoclinic collision and symmetry breaking

As has been described earlier, at band center, namely for $E = 0$, orbits of the Harper map below ϵ_c lie on invariant curves that consist of two branches (these are denoted C for central and N for noncentral in Fig. 7a). These branches originate in the fact that the mapping for $\epsilon = 0$ has a period-2 fixed point and no period-1 fixed point. Different initial points on the (x, ϕ) plane generate different invariant curves, the two branches of which are widely separated at $\epsilon=0$, but as $\epsilon \rightarrow 1$, these branches begin to approach each other. For a particular curve, the branches collide at a dense set of points, at ϵ_c , and indeed, all the different curves merge at ϵ_c to give a single attractor which has a dense set of singularities (Fig. 7b). At the merging point, the Lyapunov exponent remains zero. The distance between the two branches of a given invariant curve decreases as a power in $\epsilon_c-\epsilon$, as does the distance between any pair of invariant curves (Fig. 7c). As previously noted, the

homoclinic collision route to SNA is accompanied by a symmetry-breaking. Below ϵ_c when the Lyapunov exponent is zero, there is a quasiperiodic symmetry in the stretch exponents (Fig. 7d), and this symmetry is lost above ϵ_c , once the attractor has negative Lyapunov exponent (Fig. 7e).

While each eigenvalue at ϵ_c is associated with a SNA, not all SNAs arise from the above homoclinic collision route. Indeed, the more general route to SNA in this system appears to be related to both the blowout bifurcation as well as the so-called fractalization scenario for the formation of SNAs, and this is discussed in the following subsection.

B. Other Bifurcations and Fractalization

Given the complexity of the phase diagram for the Harper system with the hierarchical organization of SNA (S) and torus (Q,G) regions, there are a number of bifurcations as parameters are varied. For fixed ϵ below ϵ_c , there are bifurcations from 2-frequency to 3-frequency tori as E is varied, the signature of this transition being the change of the Lyapunov exponent from a negative value to zero. There is therefore a discontinuity in the slope of the Lyapunov exponent versus E curve. The 3-frequency tori (Q) densely cover the phase space, while the 2-frequency tori (G) are attractors of the dynamics (including the case when the Lyapunov exponent is exactly zero). This transition is also, therefore, accompanied by a breaking of the symmetry in the stretch exponents. On the other hand, by fixing E and varying ϵ , there are other bifurcations depending on the value of E . There can be transitions from 3-frequency tori to 2-frequency tori below ϵ_c , and from 2-frequency tori to SNA above ϵ_c .

Shown in Fig. 8a is the variation of the Lyapunov exponent with ϵ for $E = 1$; the bifurcations being signaled by a discontinuity in slope of the curve, with the Lyapunov exponent being strictly nonpositive throughout. SNAs are first formed at this energy at $\epsilon \approx 2.5200$, below which there is an attracting 2-frequency torus. This transition has some of the dynamical characteristics of the blowout bifurcation [35] both in the nature of the

attractors before (Fig. 8c) and after (Fig. 8d) the transition as well as in the manner in which the Lyapunov exponent varies. The fluctuations in the local Lyapunov exponents, as measured in the variance of the distribution, are large on the SNAs and zero on the tori. This is shown in Fig. 8b. Note that the Cantor set structure of the gaps (whose widths decay only as a power in ϵ) is reflected in the pattern of bifurcations along any typical line in the (E, ϵ) plane.

The $G \rightarrow S$ transition occurs along essentially all the boundaries of the SNA regions above ϵ_c . When approached from below, the attractor of the dynamics can be seen to gradually develop from a smooth curve to one with wrinkles on all scales: this is reminiscent of the fractalization process [32]. The blowout nature of the transition—insofar as the attractor abruptly changes its volume with intermittent “bursts”—can be seen more clearly along the line $E = 3$. In the torus region G , the dynamical map here has a single invariant curve (Fig. 9a), which develops kinks and wrinkles as ϵ is varied. The transition to SNA is at $\epsilon \approx 1.270(37567)$, when the attractor gets wrinkled enough and actually hits the boundary $x \rightarrow \infty$, Fig. 9b. This bifurcation can be clearly detected by measuring, say, the distance $\Delta = \min_n |1 - \tanh x_n|$, namely the closest point of the attractor from the boundary as a function of ϵ . As can be seen in Fig. 9c, this quantity abruptly decreases at the transition.

C. Characterization of Harper SNAs: Correlations

Principal among the measures that can be used to distinguish SNAs from morphologically similar chaotic attractors or from (regular) attractors which are similar dynamically (namely they have similar values of the Lyapunov exponent) are quantities that examine correlations on the attractors [24,36].

The autocorrelation function, which provides a quantitative measure of the extent to which dynamical properties are correlated, is defined for a dynamical variable x as

$$C(\tau) = \frac{\langle x_i x_{i+\tau} \rangle - \langle x_i \rangle \langle x_{i+\tau} \rangle}{\langle x_i^2 \rangle - \langle x_i \rangle^2} \quad (17)$$

where $i = 1, 2, \dots$ is a discrete time index, $\tau = 0, 1, \dots$ is the time shift, and $\langle \rangle$ denotes a time-average. If x is periodic then $C(\tau)$ varies between -1 and 1, regaining its initial value $C(0)$ in a periodic fashion. If x is chaotic, then $C(\tau)$ decays from its initial value of 1 to 0, around which latter value it fluctuates. On SNAs, the variables have correlation functions that do not recur exactly: $C(\tau)$ is also quasiperiodic and is nearly recurrent, oscillating between -1 and 1 (Fig. 10a).

The Fourier transform of the correlation function also shows these differences as characteristic spectra. The Fourier transform of a discrete sequence $\{x_k\}$ is

$$T(\Omega, N) = \frac{1}{N} \sum_{k=1}^N x_k \exp(i2\pi k\Omega), \quad (18)$$

the power spectrum being

$$P(\omega) = \lim_{N \rightarrow \infty} \langle |T(\omega, N)|^2 \rangle. \quad (19)$$

A chaotic signal typically has a continuous power spectrum, but for SNAs, the Fourier spectrum reflects the fact that the dynamics is neither chaotic nor regular, and the power spectrum consists of several peaks at frequencies corresponding to the quasiperiodicity in the dynamics; see Fig. 10b.

D. Phase Sensitivity Properties

Pikovsky and Feudel [24] introduced the phase-sensitivity exponent in order to characterize the strangeness of a attractor. This quantity measures the sensitivity of the dynamics with respect to change of phase of the external force. Given a map

$$\begin{aligned} x_{n+1} &= f(x_n, \theta_n) \\ \theta_{n+1} &= \theta_n + \omega \mod 1, \end{aligned} \quad (20)$$

the maximal value of the derivative $\partial x / \partial \theta$ can provide a suitable tool to distinguish between strange and nonstrange geometry. Since the above derivative changes along the trajectory $(x_0, \theta_0), (x_1, \theta_1), (x_2, \theta_2), \dots$, one can get a relation

$$\begin{aligned}
S_N &= \frac{\partial x_{n+1}}{\partial \theta} \\
&= f(x_n, \theta_n) + f(x_n, \theta_n) \frac{\partial x_n}{\partial \theta}
\end{aligned} \tag{21}$$

where S_N is the derivative with respect to external phase (we follow the notation of Pikovsky and Feudel [24]). The number of maxima in S_N up to time N is

$$\gamma_N(x, \theta) = \max_{0 \leq n \leq N} |S_n|. \tag{22}$$

The value of γ_N grows with N , a consequence of the fact that the attractor is not smooth; see Fig 11a. Also, as Pikovsky and Feudel [24] noted, the growth rate of the partial sum with time represent the strangeness of attractor, so it becomes necessary to calculate the minimum value of $\gamma_N(x, \theta)$ with respect to randomly choose initial points,

$$\Gamma_N = \min_{x, \theta} \left[\max_{0 \leq n \leq N} |S_n| \right]. \tag{23}$$

From Fig. 11b we see that $\Gamma_N \sim N^\mu$, where μ is the so-called phase sensitivity exponent. If the attractor is smooth (i.e. nonfractal) then the maximum derivative with respect to external phase is bounded, and this value saturates as a function of iteration. However, in the case of SNAs, the maximum derivative with respect to external phase increases indefinitely with iteration.

V. MAPS OF HARPER TYPE

In this section we discuss the dynamics of mappings similar to Eqs. (5-6). The Harper map can be generalized in two essentially different ways. By generalizing the potential in the Harper equation but retaining the feature of quasiperiodicity, one essentially obtains other Schrödinger equations. Power-law localization is known to occur in a variety of quasiperiodic systems, well studied examples being the potentials [37]

$$V_n = \epsilon_1 \cos 2\pi n\omega + \epsilon_3 \cos 6\pi n\omega \tag{24}$$

and

$$V_n = \frac{\epsilon}{\tanh \mu} \tanh(\mu \cos 2\pi n\omega). \quad (25)$$

In both these systems, it is known that there are mobility edges. In the resulting maps, which are very similar to the Harper, the cosine “driving” term is replaced by a more general function which is also quasiperiodic since ω is irrational.

Since both these above cases can be viewed as modifications of the Harper system, the phase diagrams obtained by variation of E and the parameters (ϵ_1, ϵ_3 or ϵ, μ) are quite similar to Fig. 3a,b. Some instances have been studied previously. For Eq. (24) with $\epsilon_3 = 1/4$, the regions of 3– and 2–frequency tori are arranged in a manner very similar to the case with $\epsilon_3 = 0$, namely the Harper map (Fig. 3a), except that the transition from extended to localized states does not occur on the line $\epsilon_1 = 1$, but instead on some complicated curve in the (E, ϵ_1) plane; see Fig. 12a. Fig. 12b shows the corresponding phase diagram for the potential in Eq. (25).

A number of quasiperiodic potentials generated from abstract sequences support critical states [20]. Among the most extensively studied such sequences is the Fibonacci chain, the potential for which is defined by

$$\begin{aligned} V_n = \alpha & \quad 0 \leq \{n\omega\} \leq \omega \\ & = -\alpha \quad \omega < \{n\omega\} \leq 1. \end{aligned} \quad (26)$$

For any value of α , all states of this system are critical [37–40]. The corresponding Schrödinger equation can be transformed to the mapping

$$x_{k+1} = -[x_k - E + V_k]^{-1} \quad (27)$$

with V_k given by Eq. (26). Analogous maps can be obtained for the Thue–Morse, Rudin–Shapiro and period–doubling quasiperiodic sequences, and these have been shown to support SNAs [27]. The nature of the eigenspectrum in such cases will be discussed elsewhere [28].

Another possible generalization of the Harper map gives

$$x_{k+1} = -[f(x_k) + 2\epsilon \cos 2\pi \phi_k]^{-1} \quad (28)$$

$$\phi_{k+1} = \phi_k + \omega \quad \text{mod } 1. \quad (29)$$

where $f(x)$ is now arbitrary while the quasiperiodic driving term is retained. Because of the somewhat unusual nature of the mapping, not much can be said in general—there can now be chaotic motion as well if f is not 1–1, for example. However, analysis of the strong-coupling limit still suggests that SNAs should arise in such systems. Indeed, for special cases that have been examined so far [25,31] many of the scenarios to SNA that have been seen in the Harper mapping also exist in these more general cases. An important limitation is that except for the case when f is linear, the above mapping cannot arise from a Schrödinger equation, and thus the parallel insights that derive from study of the quantum-mechanical system are not available for nonlinear $f(x)$.

VI. SUMMARY AND DISCUSSION

In the present work we have studied the Harper equation from a dynamical systems point of view. The correspondence between localized states and strange nonchaotic attractors [18,22] makes it possible to obtain a number of properties of the eigenspectrum, as well as the eigenstates of the Harper equation through a study of the equivalent iterative Harper map.

For the spectral gaps, we have described a labeling scheme which explicitly connects the number-theoretic properties of ω with the gap ordering. This is most conveniently depicted on a Cayley tree, which we describe in detail for the case of the so-called silver-mean quadratic irrational $\omega = \sqrt{2} - 1$. The general principles governing this organization are not difficult to ascertain, and computationally, these are most easily deduced through examination of the orbits of the Harper map. The gap indices that we obtain are related to the winding numbers introduced earlier by Johnson and Moser [41], and these (integer) indices determine the scaling behaviour of the gaps as a function of the coupling. We find that the width of each gap decreases only as a power of the coupling, and thus the gaps never close: this confirms the conjecture of Thouless *et al.* [33]. The organization of the gaps on the Cayley tree also makes it possible to identify other scaling properties. For fixed

ϵ , the widths of gaps along a branch of the tree also show a power-law scaling in the gap indices.

The transition from extended to localized states is accompanied by a breaking of the symmetry of *stretch exponents* [25]. This symmetry-breaking appears to accompany a number of the bifurcations in this system. Recall that the stretch exponents are the logarithms of the ratio of wavefunctions at adjacent sites. Thus the symmetry that gives a zero value of the Lyapunov exponent in the extended state is the following: the ratio of the wavefunctions at a triple of sites, $i-1, i, i+1$, (a:b:c, say) is such that at the triple of sites $j-1, j, j+1$, the ratio of wavefunctions is (approximately, because of the quasiperiodicity) reversed (namely c:b:a), for each j such that $j-i$ is a Fibonacci number. On the other hand, the wavefunctions of the localized phase do not have this symmetry and are instead characterized through their multifractal oscillations, which have also been extensively studied [42].

There have been several realizations of the Harper system in experiments. Experiments of wave-chaos in microwave scattering [43] in a geometry that is designed to mimic the Harper equation have shown the Hofstadter butterfly. In a very recent experimental study of the Hall conductance of a suitably designed heterostructure [44], the Cantor-set nature of the energy spectrum has been explicitly detected. The scaling results for the gaps reported in this paper and elucidation of the gap organization are relevant to such studies.

The methods of analysis employed here have wide applicability. A number of quasiperiodic systems in 1-dimension are known to have singular continuous spectra. The correspondences studied here for the Harper system appear to be valid in the general cases as well, and thus offer an alternate and powerful means of analyzing such problems.

ACKNOWLEDGMENT

This work is supported by a grant from the Department of Science and Technology. We thank Prof. Jean Bellisard for very helpful correspondence on the spectral gaps of the Harper equation.

REFERENCES

- [1] P. G. Harper, Proc. Phys. Soc. London A **68**, 874 (1955).
- [2] C.M Soukoulis and E. N. Economou, Phys. Rev. Lett. **48**, 1043 (1982).
- [3] A.G. Abanov, J.C. Talstra, P.B. Wiegmann, Phys. Rev. Lett. **81**, 2112 (1998).
- [4] D. R. Hofstadter, Phys. Rev. B **14**, 2239 (1976).
- [5] M. Hilke, J. Phys. A **30**, L367 (1997).
- [6] P. B. Wiegmann Prog. Theor. Phy. Suppl. **134**, 171 (1999).
- [7] M. Wilkinson and R. J. Kay, Phys. Rev. Lett. **76**, 1896 (1996).
- [8] P.W. Anderson, Phys. Rev. **109**, 1492 (1958); Rev. of Mod. Phys. **50**, 191 (1978).
- [9] N. F. Mott, *Metal-Insulator Transitions*, (Taylor and Francis, London 1990).
- [10] M. Ya. Azbel, Sov. Phys. JETP, **19**, 634 (1964); Phys. Rev. Lett. **43**, 1954 (1979).
- [11] R. del Rio, S. Jitomirskaya, Y. Last, and B. Simon, Phys. Rev. Lett. **75**, 117 (1995).
- [12] J. B. Sokoloff, Phys. Rep. **126**, 189 (1985).
- [13] S. Y. Jitomirskaya and Y. Last, Phys. Rev. Lett. **76**, 1765 (1996).
- [14] D. J. Thouless, J. Phys. C **5**, 77 (1972).
- [15] T. Geisel, R. Ketzmerick, G. Petschelt, Phys. Rev. Lett. **66**, 1651 (1991).
- [16] J. Sun, Phys. Rev. B **40**, 8270 (1989).
- [17] G. André and S. Aubry, Ann. Isr. Phys. Soc., **3**, 133 (1980).
- [18] A. Bondeson, E. Ott, and T. M. Antonsen, Phys. Rev. Lett. **55**, 2103 (1985).
- [19] C. Grebogi, E. Ott, S. Pelikan, and J. Yorke, Physica D **13**, 261 (1984).
- [20] J. M. Luck, Phys. Rev. B **39**, 5834 (1989).

- [21] J. Ketoja and I. Satija, Phys. Rev. Lett. **75**, 2762 (1995).
- [22] J. Ketoja and I. Satija, Physica D **109**, 70 (1997).
- [23] A. Prasad, S. S. Negi, and R. Ramaswamy, Int. J. Bifurcation and Chaos, to be published (2001).
- [24] A. Pikovsky and U. Feudel, Chaos, **5**, 253 (1995).
- [25] A. Prasad, R. Ramaswamy, I. Satija, and N. Shah, Phys. Rev. Lett. **83**, 4530 (1999).
- [26] S. S. Negi and R. Ramaswamy, to be published.
- [27] S. S. Negi and R. Ramaswamy, Pramana J. Phys., **56**, 47 (2001).
- [28] S. S. Negi and R. Ramaswamy, to be published.
- [29] J. Heagy and W. L. Ditto, J. Nonlin. Sci., **1**, 423 (1991).
- [30] A. Prasad and R. Ramaswamy, Phys. Rev. E **60**, 2961 (1999) and references therein.
- [31] S S Negi, Ph D thesis, Jawaharlal Nehru University, New Delhi.
- [32] K. Kaneko, Prog. Theor. Phys. **72**, 202 (1984).
- [33] D. J. Thouless, M. Kohmoto, M. P. Nightingale, and M. den Nijs, Phys. Rev. Lett. **49**, 405 (1982)
- [34] A. Ya. Khinchin, *Continued Fractions*, (University of Chicago press, 1964).
- [35] T. Yalçinkaya and Y. C. Lai, Phys. Rev. Lett. **77**, 5039 (1996).
- [36] A. Pikovsky and U. Feudel, J. Phys. A **27**, 5209 (1994).
- [37] M. Kohmoto, Phys. Rev. Lett. **51**, 1198 (1983).
- [38] H. Hiramoto and M. Kohmoto Phys. Rev. B **40**, 8225 (1989).
- [39] M. Kohmoto, L. P. Kadanoff, and C. Tang, Phys. Rev. Lett. **50**, 1870 (1983).

[40] S. Ostlund, R. Pandit, D. Rand, H. J. Schellnhuber, and E. D. Siggia, Phys. Rev. Lett. **50**, 1873 (1983).

[41] R. Johnson and J. Moser, Commun. Math. Phys., **84**, 403 (1983).

[42] H. Hiramoto and M. Kohmoto, Int. J. Mod. Phys. B**6**, 281 (1992)

[43] H.J. Stockmann, *Quantum Chaos : An Introduction*, (Cambridge University Press, Cambridge, 1999).

[44] C. Albrecht, J. H. Smet, K. von Klitzing, D. Weiss, V. Umansky, and H. Schweizer, Phys. Rev. Lett. **86**, 147 (2001).

Figure Captions

Fig. 1. (a) Lyapunov exponent versus energy at ϵ_c for $\omega = (\sqrt{5}-1)/2$. Gap labels are indicated for the largest visible gaps. At every bifurcation, when $\lambda = 0$, the dynamics is on a SNA. (b) Lyapunov exponent versus energy at ϵ_c for $\omega = \sqrt{2} - 1$. Gap labels are indicated, as in Fig. 1a, for the largest visible gaps.

Fig. 2. Lyapunov exponent versus ϵ for the eigenvalue $E = 0$. The extended to localized transition occurs at $\epsilon = \epsilon_c = 1$.

Fig. 3. (a) Phase diagram for the Harper map for $\omega = \sqrt{2} - 1$. Below ϵ_c , namely the vertical line the dynamics is on three-frequency quasiperiodic (Q) orbits or extended states, 1-d attractors which are two-frequency quasiperiodic orbits or gaps (G), and above ϵ_c , the dynamics is on SNAs (S), and 1-d attractors (G). Only the largest gaps are visible at this scale.

(b) Detail in the neighborhood of the central gaps. Every tongue of SNAs necessarily has a similar structure.

Fig. 4. (a) Ordering of the gaps for $\omega = (\sqrt{5}-1)/2$, the golden mean ratio. Only part of the Cayley tree described in the text is shown for clarity. Each node has two daughters except for 0, which has only one.

(b) The corresponding Cayley tree for the case of ω the silver mean, $\sqrt{2} - 1$.

Fig. 5. The attractor for a value of E corresponding to the gap $N = 8$. Note that the orbit has 8 branches that traverse the range $-\infty < x < \infty$.

Fig. 6. Scaling of the gap widths, w_N (\bullet), and depths d_N (\diamond) as a function of gap index, N , at $\epsilon = \epsilon_c$ for the cases of (a) $\omega = (\sqrt{5}-1)/2$ and (b) $\omega = \sqrt{2} - 1$. For clarity, the depths have been multiplied by a factor of 10. The dashed line fitting the depths has slope -1. The dotted lines show the scaling of the two families of gaps; see the text for details.

Fig. 7. (a) Invariant curve for the Harper map corresponding to the band center extended state, the central and noncentral branches being indicated by C and N respectively. (b) The fractal attractor corresponding to the critically localized state. (c) Scaling of the minimum vertical distance d between a family of different invariant curves in the Harper map as a function of the parameter $(1 - \epsilon)$ for the eigenvalue $E = 0$. Different pairs of curves approach each other at different rates, but at ϵ_c , *all* curves collide to form the critical SNA. (d) First return map for the stretch exponent showing the quasiperiodic symmetry below ϵ_c , and (e) the return map above ϵ_c , when this symmetry is broken.

Fig. 8. The depressed blowout bifurcation along the line $E = 1$. (a) Variation of the Lyapunov exponent with ϵ for ω the golden mean. (b) Fluctuations of the Lyapunov exponent. The attractor (c) before (a two-frequency torus) and (d) after (a SNA) the bifurcation.

Fig. 9. The bifurcations along the line $E = 3$, showing the attractor (a) before ($\epsilon = 1.270375\dots$) and (b) after the $G \rightarrow S$ transition. (c) The distance from the attractor to the boundary as a function of ϵ .

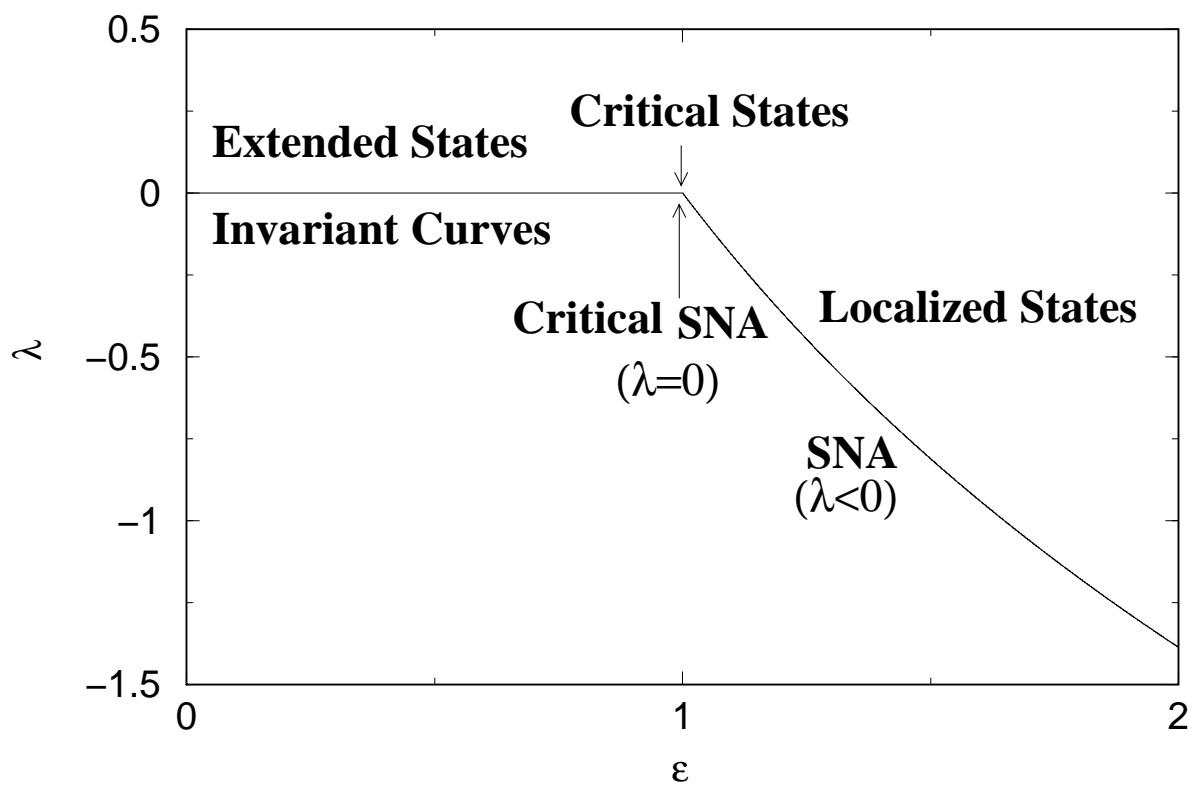
Fig. 10. For the $E = 0$ critical SNA for ω the golden mean (a) the correlation function, and (b) the power spectrum.

Fig. 11. (a) Maxima of the partial sum γ_N (cf. Eq. (22)) on the critical SNA at $\epsilon_c, E=0$ in the Harper map, as a function of iteration length, N . (b) Γ_N , the minimum value of γ_N .

Fig. 12. Phase diagram for (a) the generalized Harper model, Eq. (24) with $\epsilon_1 =$ and ϵ_3 . The tongue-like regions where SNAs can be found continue to be hierarchically arranged but the transition from localized to extended states occurs along a curve in the plane rather than on the line $\epsilon=1$. (b) As in Fig. 12(a) for the potential of Eq. (25).

This figure "fig1.gif" is available in "gif" format from:

<http://arxiv.org/ps/nlin/0105035v1>

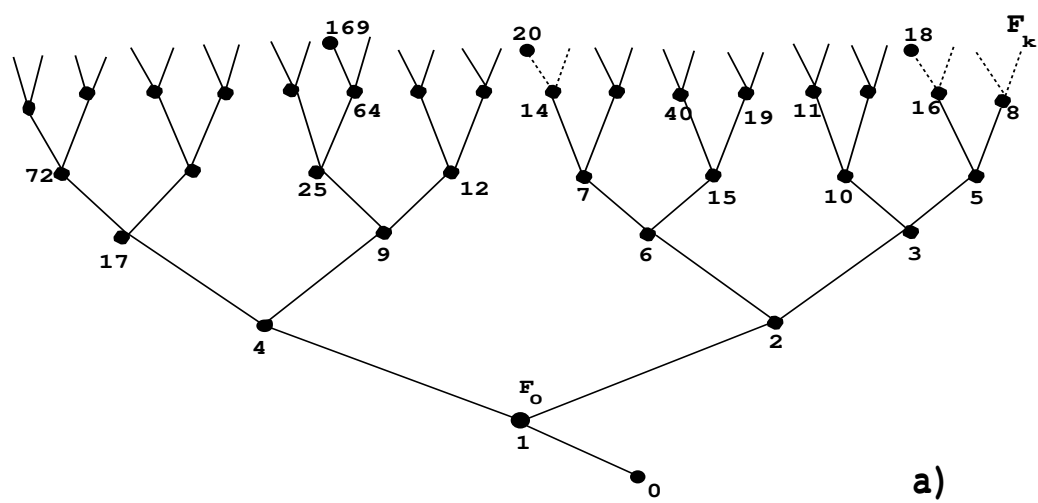


This figure "fig3a.gif" is available in "gif" format from:

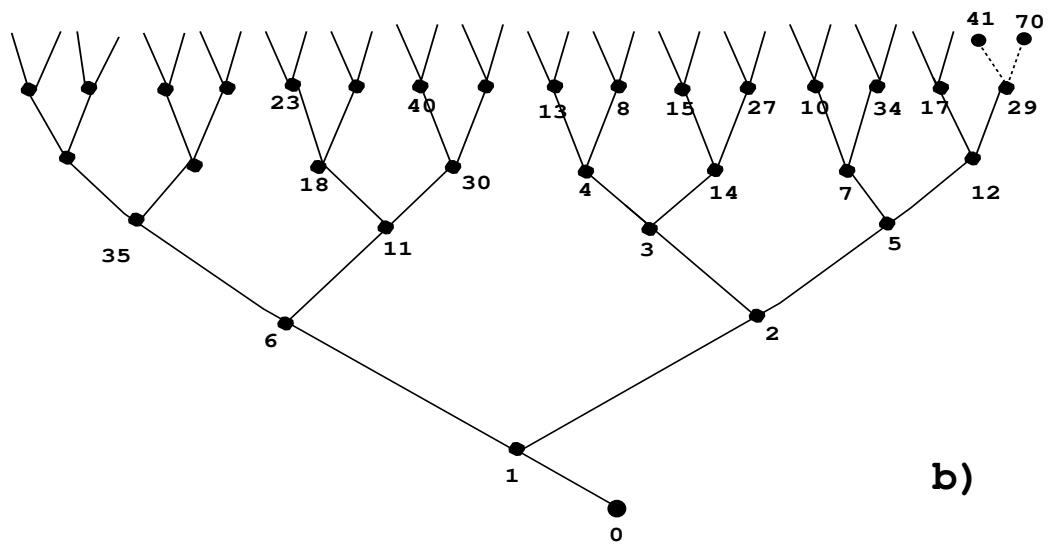
<http://arxiv.org/ps/nlin/0105035v1>

This figure "fig3b.gif" is available in "gif" format from:

<http://arxiv.org/ps/nlin/0105035v1>



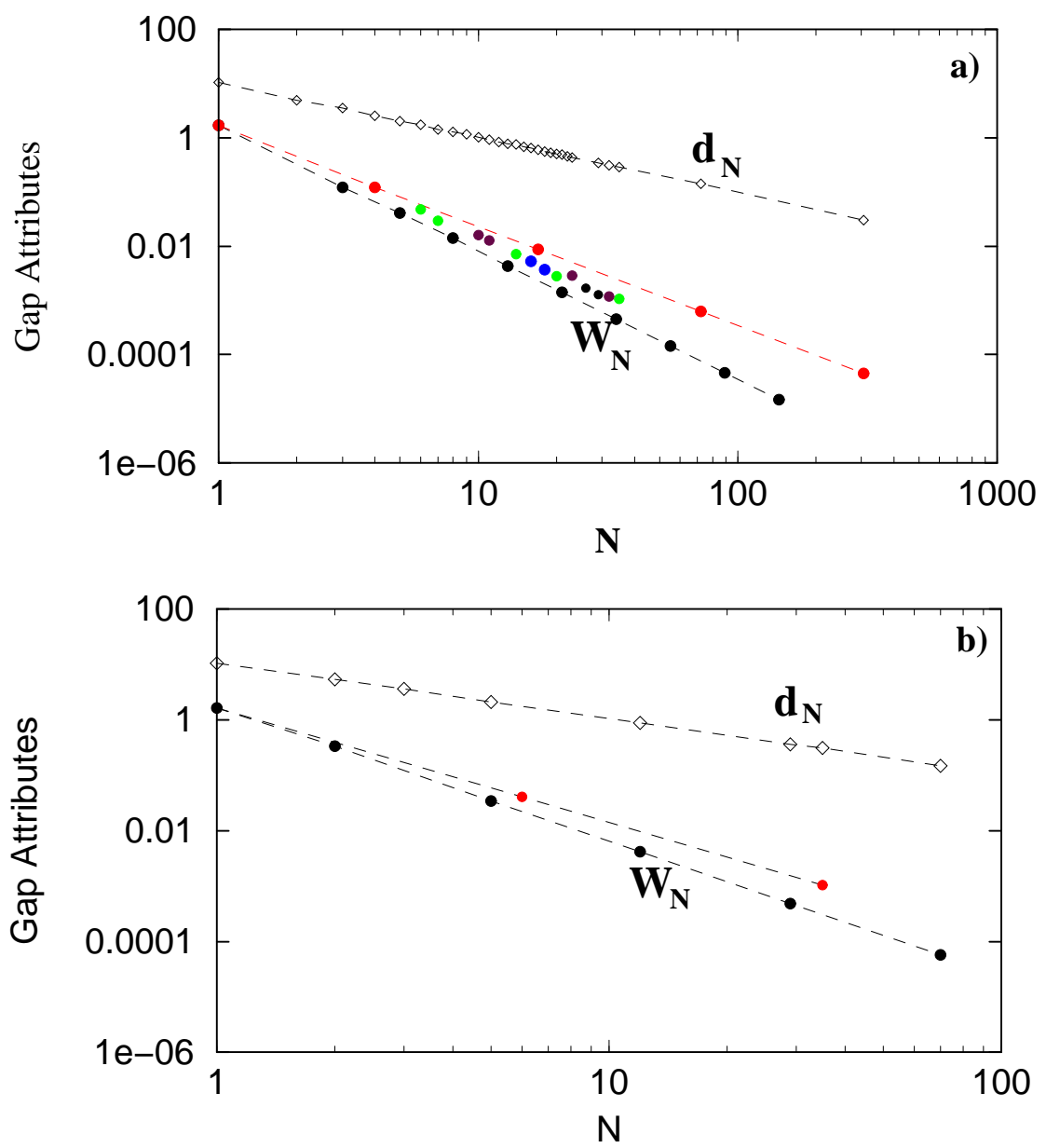
a)



b)

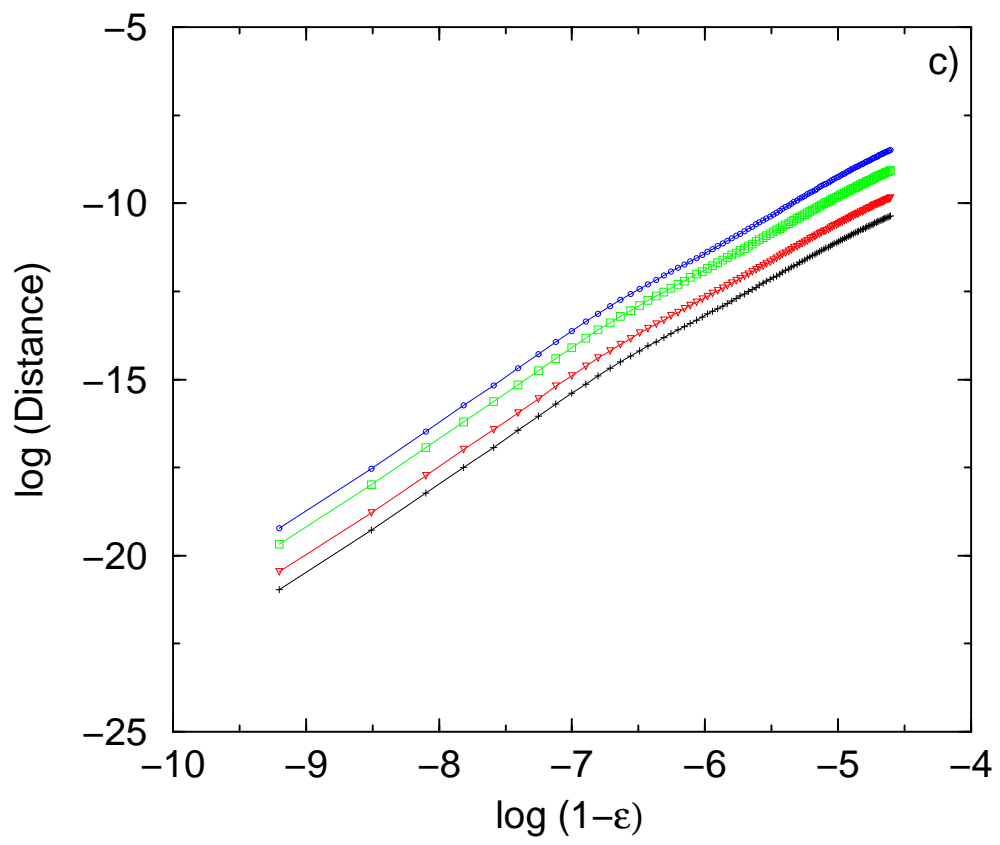
This figure "fig5.gif" is available in "gif" format from:

<http://arxiv.org/ps/nlin/0105035v1>



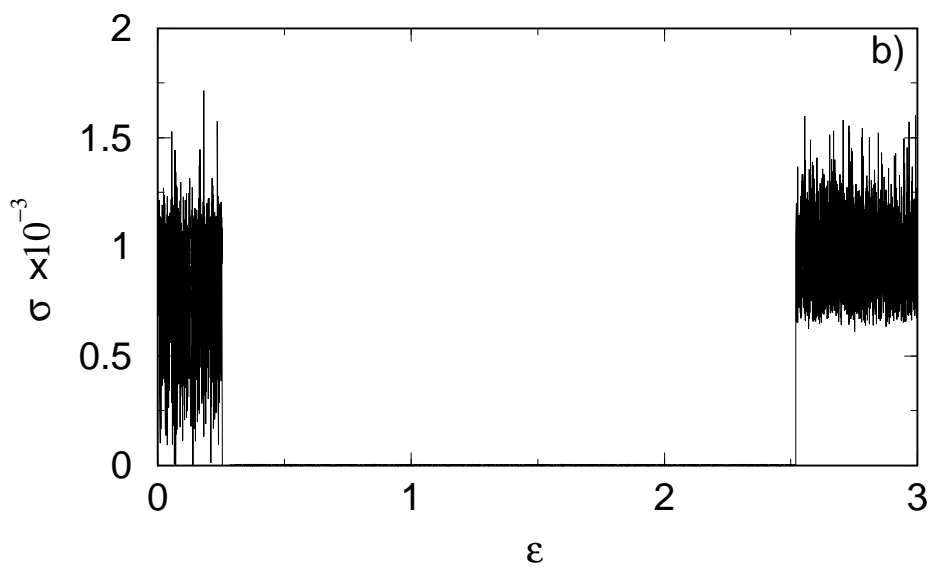
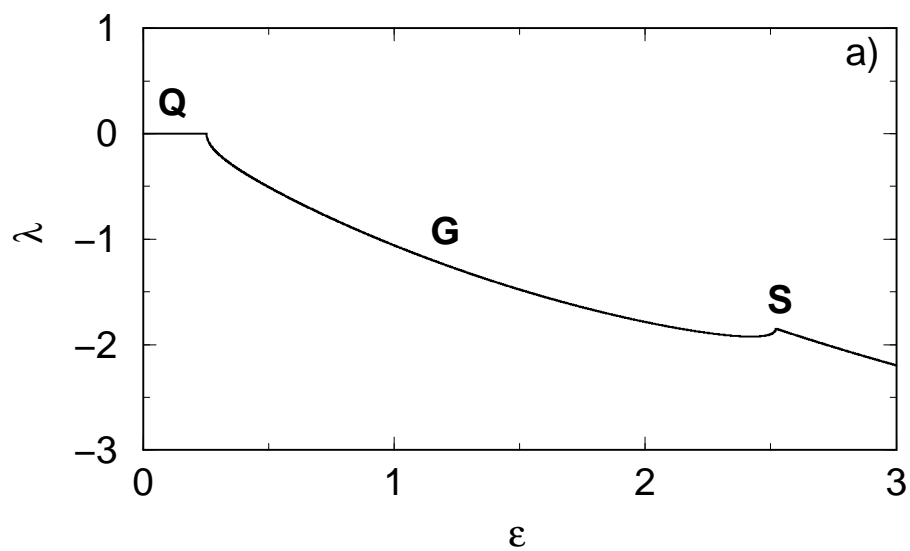
This figure "fig7ab.gif" is available in "gif" format from:

<http://arxiv.org/ps/nlin/0105035v1>



This figure "fig7de.gif" is available in "gif" format from:

<http://arxiv.org/ps/nlin/0105035v1>

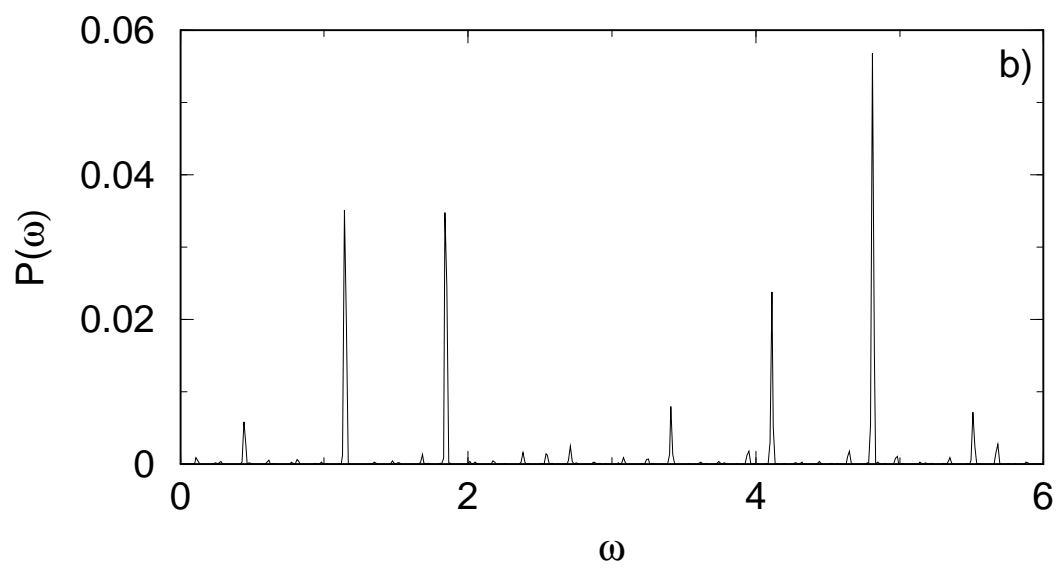
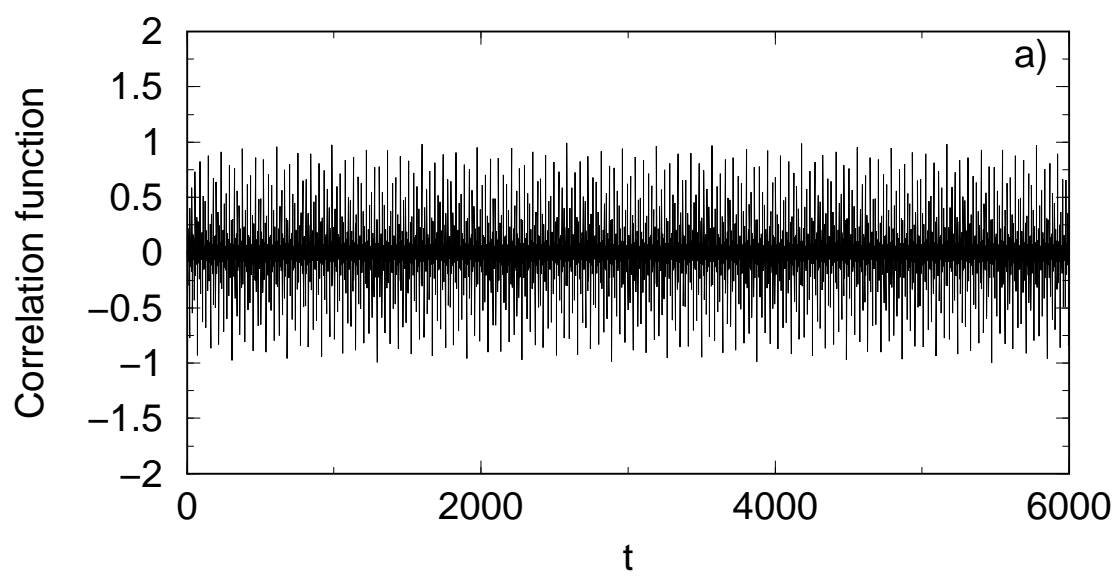


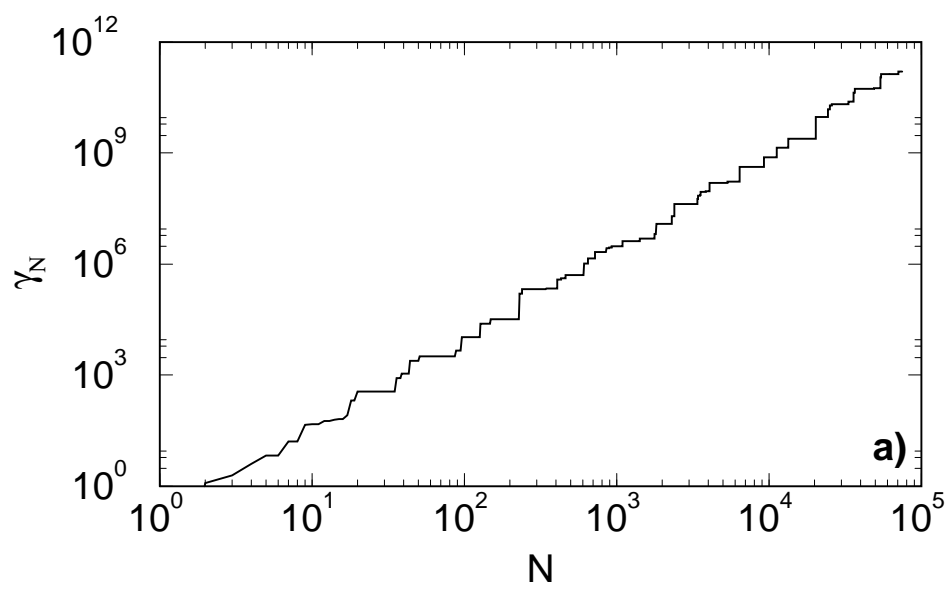
This figure "fig8b.gif" is available in "gif" format from:

<http://arxiv.org/ps/nlin/0105035v1>

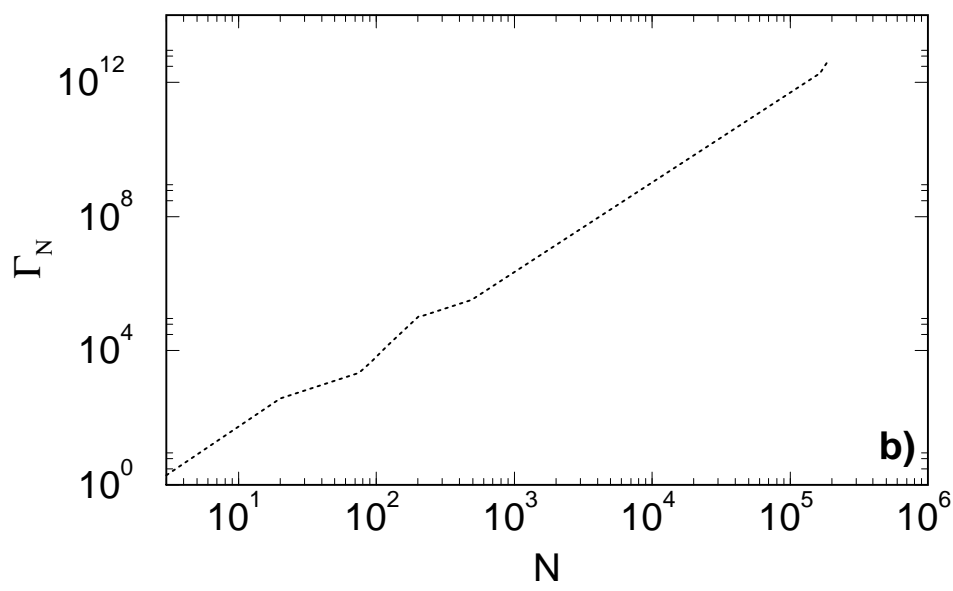
This figure "fig9.gif" is available in "gif" format from:

<http://arxiv.org/ps/nlin/0105035v1>





a)



b)

This figure "fig12a.gif" is available in "gif" format from:

<http://arxiv.org/ps/nlin/0105035v1>

This figure "fig12b.gif" is available in "gif" format from:

<http://arxiv.org/ps/nlin/0105035v1>